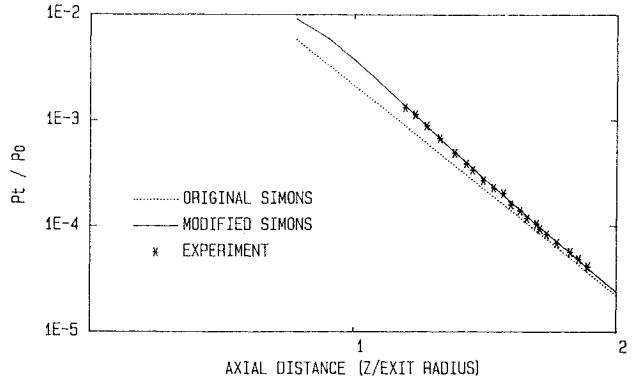

Fig. 1 Pitot pressure distributions along the plume axis for the expansion of nitrogen through the MBB/ERNO 0.5N thruster.

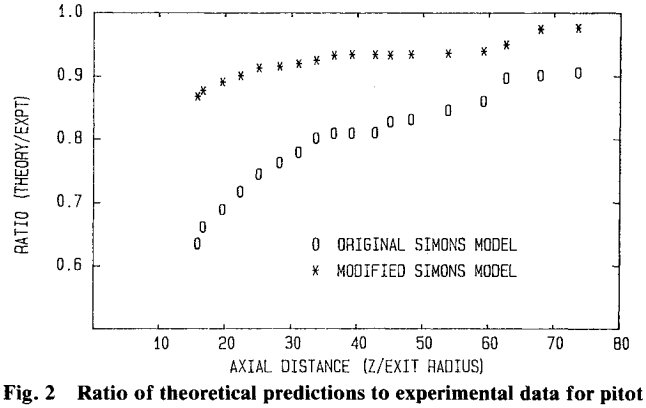

Fig. 2 Ratio of theoretical predictions to experimental data for pitot pressure distribution along the axis for the expansion of argon.

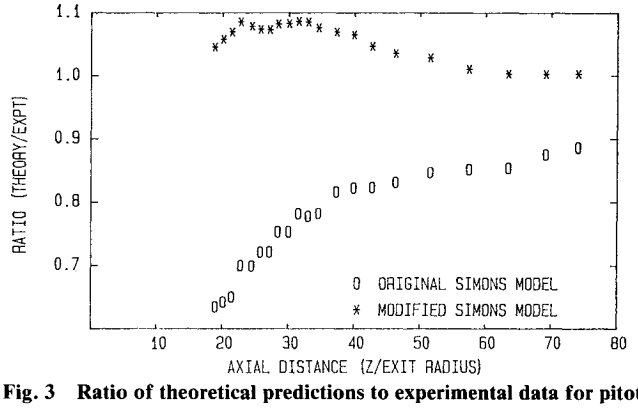

Fig. 3 Ratio of theoretical predictions to experimental data for pitot pressure distribution along the axis for the expansion of tetrafluoromethane.

again it is clear that the expressions derived for the expansion of nitrogen are usefully applied to the polyatomic gas.

It is interesting to compare Figs. 2 and 3. In the case of the monatomic gas, the use of Eqs. (3) tends to just overestimate the pitot pressure in comparison with experiment. On the other hand, when γ is much less than 1.4, the results are underestimated by the theoretical predictions. If such behavior is confirmed by further comparison with experimental data, then it may be possible to derive an improved form of Eqs. (3) as a function of the specific heat of the gas.

In Ref. 4 it was possible to define the nozzle exit conditions under which the use of the modified Simons model is preferred to the original formulation. The criterion employed was a divergence in axial density of 10% for the two methods, and was expressed as a function of exit Mach number and nozzle exit half-angle. For the expansion of monatomic and polyatomic gases, and also for gas mixtures, it is suggested that the decision be made with reference to an exit Mach number obtained with $\gamma = 1.4$ together with the exit half-angle and the usage criterion chart shown in Ref. 4.

Table 1 Nozzle conditions investigated

Test gas	N_2	Ar	CF_4
Molecular weight	28	40	88
Ratio of specific heats	1.40	1.67	1.17
Boundary-layer thickness, %	34	35	27
Mach number	5.09	7.23	3.96
Plume constant	3.39	6.78	0.93

It is perhaps surprising that Eqs. (2) and (3), which were derived from a diatomic gas, should be so effective when applied to monatomic and polyatomic molecules. The physical explanation for the nonradial behavior lies in the fact that the nozzle exit conditions are markedly different from those for an effusive source. It is shown in Ref. 4 that the form of Eqs. (3) is at least quantitatively correct.

Conclusions

The nonradial density decay observed experimentally in jets of nitrogen, argon, and tetrafluoromethane has been successfully predicted using the Modified Simons model. Calculations made with this simple analytical model offer significant improvement on the results obtained with Simons original formula. It is therefore proposed that the Modified Simons model may be applied with some confidence to any rocket or thruster plume that may be expected to exhibit a significant degree of nonradial behavior.

References

[1]Boynton, F. P., "Highly Underexpanded Jet Structure. Exact and Approximate Calculations," *AIAA Journal,* Vol. 5, Sept. 1968, pp. 1143–1147.

[2]Simons, G. A., "Effect of Nozzle Boundary Layers on Rocket Exhaust Plumes," *AIAA Journal,* Vol. 10, Nov. 1972, pp. 1534–1535.

[3]Genovese, J. E., "Rapid Estimation of Hydrazine Exhaust Plume Interaction," AIAA Paper 78-1091, July 1978.

[4]Boyd, I. D. and Stark, J. P. W., "Modification of the Simons Model for Calculation of Nonradial Expansion Plumes," *Proceedings of the 16th International Symposium on Rarefied Gas Dynamics,* AIAA, Washington, DC, 1989.

[5]Legge, H., Dankert, C., and Dettleff, G., "Experimental Analysis of Plume Flow From Small Thrusters," *Proceedings of the 14th International Symposium on Rarefied Gas Dynamics,* University of Tokyo Press, Tokyo, Japan, Vol. 1, 1984, pp. 279–286.

[6]Boyd, I. D. and Stark, J. P. W., "Modeling of Small Hydrazine Thruster Plumes Using Discrete Particle and Continuum Methods," AIAA Paper 88-2631, June 1988.

[7]Dettleff, G., "Experimental Verification of Rocket Exhaust Plumes and Impingement Effects on Spacecraft Surfaces," Deutsche Forschungs und Versuchsanstalt für Luft und Raumfahrt, Göttingen, FRG, Report IB 222-84 A42, 1984.

Further Investigations of Fracture Toughness Measurement Using Numerical-Experimental Technique

Wen-Hwa Chen* and Kuen-Tsann Chen†
National Tsing Hua University
Hsinchu, Taiwan, Republic of China
and
Jeun Heh‡
Army Research and Development Center
Taichung, Taiwan, Republic of China

Introduction

THE theory of elastic-plastic fracture mechanics has been widely employed for efficient and reliable design of struc-

Received Jan. 9, 1989; revision received March 15, 1989.

*Professor, Department of Power Mechanical Engineering.
†Graduate Student, Department of Power Mechanical Engineering.
‡Director.

tures in recent years. Two different approaches are usually adopted to describe the ductile fracture behaviors of cracked structure. The first approach is based on experimental techniques, and the measurement of fracture toughness J_{IC} is essential. In literature, the standard test procedures of fracture toughness J_{IC} have been well documented.[1,2] However, to measure the fracture toughness J_{IC} for ductile metals,[2] unavoidable plastic deformation or necking near the crack-tip is observed. This may affect the J_{IC} value measured. Besides, the accuracy of the experimental data is also governed by other factors, such as specimens and environmental conditions, etc. Thus, an appropriate verification work is needed, especially for new materials.

The second approach is numerical analysis. Because of the great versatility in dealing with complicated geometric and material behaviors, the application of the finite-element method to compute the J integral of elastic-plastic cracked structures has been done by many researchers.[3,4] However, the instability point of crack initiation, and thus J_{IC}, needs to be determined by experiment.

The aim of this work is, therefore, to construct an accurate hybrid numerical-experimental technique for determining the fracture toughness J_{IC}. The formulas adopted for measuring the J_{IC} value in ASTM standard test method[2] are corrected. The improvement of the accuracy of the determined J_{IC} value can be noted as compared with solutions obtained by an incremental hybrid displacement finite-element procedure for elastic-plastic fracture mechanics analysis.[3,4]

Material, Specimen, and Testing

The material of S17C grade-A steel is used here. The mechanical properties are tested by Instron 1322 servohydraulic testing system at room temperature (25°C), and the average tensile behaviors are given as follows: yielding strength $\sigma_y = 297.0$ MPa, ultimate strength $\sigma_u = 455.6$ MPa, effective yield strength $\sigma_{ys} = 376.3$ MPa, and Young's modulus $E = 221.1$ GPa.

In accordance with ASTM standard,[2] all the compact specimens are machined to satisfy the following requirements:

$$B \text{ or } b > 25\,(J_{IC}/\sigma_{ys}) \tag{1}$$

As shown in Fig. 1, B is the thickness of specimen, $b(=W-a_0)$ is the initial uncracked ligament, W is the specimen width, and a_0 is the original crack length. There are two sets of specimens with thicknesses of 17 and 27 mm. Each machined specimen is precracked by a range of 1.5–15KN cyclic loading. The frequency of cyclic loading taken is 2 Hz. The average number of cycles needed for precracking is about 60,000.

Following ASTM standard procedure,[2] each precracked specimen is first loaded with a stroke control at 0.005 mm/s until a desired crack extension Δa is reached and then unloaded. As shown in Fig. 1, to distinguish the front of crack propagation, a postcracking fatigue process must be performed at a slow crack growth rate.

Experimental Results

Based on the experimental data, the J integral for elastic-plastic cracked structures can be evaluated by[2]

$$J = f(a0/W) \tag{2}$$

where A is the area under the load/load line displacement curve and $f(a_0/w)$ is a dimensionless coefficient value that corrects for the tensile component of loading.[2] The calculated crack extension Δa (see Fig. 1) and corresponding J value are used to plot the J — Δa resistance curve. Figure 2 shows the obtained J — Δa curves for specimens of different thickness, respectively.

To determine the J_{IC} value, according to ASTM standard,[2] the equation of blunting line, $J = 2\sigma_{ys}\Delta a$, is constructed. The intersection of the J — Δa curve and the blunting line defines the point of crack initiation, where the J_{IC} value is measured. The J_{IC} values obtained from Fig. 2 are 54.3 and 54.9 N/mm for thicknesses 17 and 27 mm, respectively. Those stable data also reveal that the J_{IC} value is indeed thickness-independent.

Elastic-Plastic Finite-Element Analysis

Based on the developed incremental hybrid displacement finite-element model for elastic-plastic fracture mechanics analysis,[3,4] the J integral for the compact specimen is computed. The finite-element mesh of one-half of the specimen employed in the analysis is shown in Fig. 3. Four six-node sector-shaped singular elements are employed to model the region around the crack-tip, and 26 eight-node quadratic isoparametric elements are adopted for modeling of the specimen. Three independent variables, say, element interior

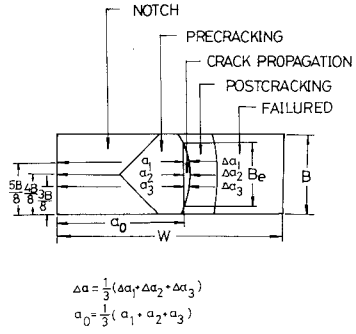

Fig. 1 Cross section of the specimen.

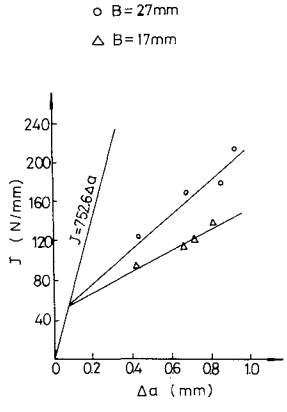

Fig. 2 J—Δa resistance curve.

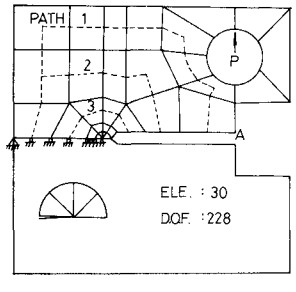

Fig. 3 Finite-element mesh of compact tension specimen.

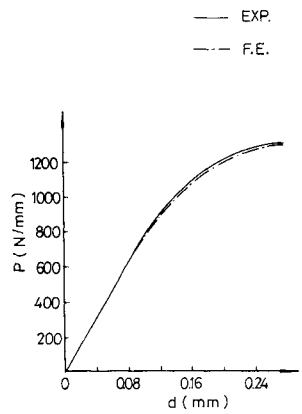

Fig. 4 Load/load line displacement curve.

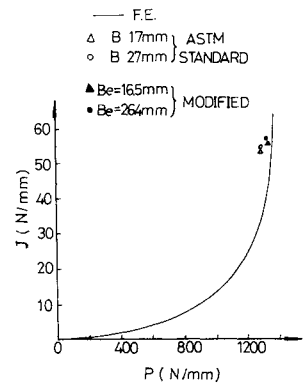

Fig. 5 *J*—*P* relation.

displacement, interelement boundary displacement, and interelement boundary tractions, are assumed. The proper singularities of stresses are embedded in the singular elements, and the interelement compatibility between the singular element and the quadratic isoparametric element is satisfied through the use of a Lagrangian multiplier technique.[3,4] Based on the concept of Saint Venant's principle[5] and numerical experiments, the pin load is treated as a concentrated load. Three integration paths around the crack-tip are selected for computing the J integral and are displayed in Fig. 3. The relations between the applied load and the load line clip gage displacement are described in Fig. 4. The experimental results are in good agreement with those obtained by finite-element analysis. The curve computed by finite-element analysis between the J integral and the applied load per unit thickness of the specimen is illustrated in Fig. 5.

Modification and Discussion

For comparison purposes, the J_{IC} values determined by ASTM standard[2] as seen in Fig. 2 are also shown in Fig. 5. It is noted that those J_{IC} values are determined based on the assumption that the crack-front is located in the area of plane strain situation.[2] However, as shown in Fig. 1, significant plastic deformation or necking without crack extension often occurs on both upper and bottom surfaces. That is, near the upper and bottom surfaces of the specimen, there will be a state of deformation closer to plane stress than plane strain. Hence, the energy required for plastic deformation needs to be taken into account. In order to correct this, the effective thickness B_e is adopted in ASTM standard formulas [e.g., Eqs. (1) and (2)] for calculating J_{IC} values instead of the specimen thickness B. The effective thickness B_e is set equal to the difference between the specimen thickness B and the thickness of plastic deformation. The corrected results are also shown in Fig. 5. As compared with rigorous finite-element solutions, closer J_{IC} values than those obtained from ASTM standard[2] are noted. The numerical-experimental technique established is also demonstrated for other materials with different thicknesses, such as Al-5083-0 alloy. The results are encouraging.

Conclusions

Further studies on the determination of the J_{IC} value using both experimental and finite-element analysis have been successfully made. The effective thickness B_e instead of the specimen thickness B is suggested for ASTM standard formula use. The techniques developed here are useful for determining an accurate J_{IC} value.

References

[1]"Standard Method of Test for Elastic-Plastic Fracture Toughness J_{IC}," JSME Standard S001-1981, pp. 1-31.

[2]"Standard Test Method for J_{IC}, A Measure of Fracture Toughness," ASTM Standard E 813-87, Vol. 03.01, 1988, pp. 686-700.

[3]Atluri, S. N., Nakagaki, M., and Chen, W. H., "Fracture Analysis Under Large-Scale Plastic Yielding: A Finite-Deformation Embedded Singularity, Elastoplastic Incremental Finite Element Solution," *Flow Growth and Fracture,* ASTM STP 1977, pp. 42-61.

[4]Chen, W. H., "Application of Finite Element Method to Elastic—Plastic Fracture Mechanics," *Journal of the Chinese Institute of Engineers,* Vol. 2, No. 1, 1979, pp. 1-13.

[5]Fung, Y. C., *Foundations of Solid Mechanics,* Prentice-Hall, Inc., Englewood Cliffs, NJ, 1965.

Electromagnetic-Capillary Instabilities of Liquid Cylinder: Production of Spherical Shells in Microgravity

Chuen-Yen Chow* and Michael Harvanek†
University of Colorado, Boulder, Colorado

Introduction

HOLLOW metallic spheres have many potential engineering applications. They can be sintered to form lightweight structures of high strength. Spherical shells of submillimeter size are sought as inertial confinement fusion targets. On the other hand, shells filled with gas, liquid, or solid may be used as efficient insulators, explosives, fire retardants, or temperature regulators. Many of the applications rely on great shell precision and smoothness and on the ability to produce large quantities of uniform shells at low cost.

Researchers at the Jet Propulsion Laboratory have been successfully producing spherical shells of various sizes in a ground-based laboratory using a hollow jet instability device[1] in which a molten metal is ejected from an annular nozzle to form a hollow liquid jet. When a flowing gas is passed through the core, the hollow jet becomes unstable and breaks up into drops, which under surface tension will develop into hollow spheres and solidify while moving along a drop tower. The size of the spheres is controlled by adjusting the speed of the core flow.

An alternative method proposed here is to manufacture spherical shells in a low-gravity environment using hollow metallic cylinders placed between two electrodes. When a di-

Presented as Paper 88-3729 at the First National Fluid Dynamics Congress, Cincinnati, OH, July 25-28, 1988; received Aug. 15, 1988; revision received May 22, 1989.

*Professor, Department of Aerospace Engineering Sciences. Associate Fellow AIAA.

†Research Assistant, Department of Aerospace Engineering Sciences.